

# Identification of Cause–Effect Relationships between Process Parameters and the Film Formation in the Semidry Electrode Production for Lithium-Ion Batteries

Matthias Leeb,\* Nico Schwarz, and Rüdiger Daub

Conventional electrode production for lithium-ion batteries has high energy and plant space demand, due to the high solvent content of the slurry to be processed by slot die or doctor blade coating. By using the semidry electrode production, the solvent content is reduced by more than 50% compared to the conventional electrode production, decreasing energy demand and drying length. Regarding technology readiness level, the semidry electrode production is on the pilot scale, as the basic principles have been shown. However, many unknown cause–effect correlations exist between the process parameters and the product properties. This study aims to analyze process parameter variations and their influence on the geometric, electrochemical, and mechanical properties of the electrode. An experimental design is utilized to obtain statistically relevant conclusions. It is found that the first calender gap and the roller speed influence the mass loading and the porosity of the electrode. The roller speed significantly influences the ionic resistance within the electrode, which may be attributed to the used release foil.

calendering,<sup>[3]</sup> in which high solvent contents of around 50% are used to process the electrode materials.<sup>[4]</sup> The drying and solvent recovery step contributes to almost half of the energy consumption in the production of LIB.<sup>[5]</sup> The high solvent content implies a high space requirement for the dryers and the recovery system, further increasing the production cost.<sup>[5]</sup>

To reduce the energy consumption the drying step of electrode production and thus the production cost, dry and semidry electrode production routes gain significant interest. The use of solvent can be completely eliminated,<sup>[6]</sup> or reduced.<sup>[7]</sup> Among different coating technologies, the free-standing film formation<sup>[8]</sup> and direct calendering were identified as the most promising processes.<sup>[2]</sup> Wiegmann et al. proposed a semidry electrode production process,

in which the solvent content can be reduced by  $\approx 50\%$  compared to the conventional slurry production.<sup>[7]</sup> The solid content can range from 72.5% to 77.5%, and as the solid content increases, the electrode density in the film formation increases.<sup>[7]</sup> Toward lower solid contents, the granules get too moist and stick together. Toward higher solid contents, the extrusion pressure gets too high. The coating, drying, and calendering processes are combined in this process.<sup>[9]</sup> Granules are produced from the base material using a twin-screw extruder at moderate temperatures of 60 °C. The granules are fed into the calender gap of a multiroller calender with horizontal roller alignment and coated directly onto the current collector. Through the water-based approach, binders from the conventional electrode production can be used for the semidry electrode production. The electrodes exhibited similar or improved rate performance compared to a wet-coated reference.<sup>[7]</sup>

Despite the investigations on the process qualification of semidry electrode production and the electrochemical advantages compared to wet-coated electrodes,<sup>[10]</sup> there are still cause–effect relationships between process parameters and electrode properties in the film formation step to be analyzed. This is a prerequisite to scale up the semidry production process and achieving desired product properties. Relevant process parameters that influence the electrode properties independent of other influences can be identified using a statistical analysis.<sup>[11]</sup> This was demonstrated for electrode production<sup>[12,13]</sup> as well as for the calendering process.<sup>[14]</sup> The identification of important influencing factors is essential to understand the semidry electrode production process. The process understanding provides a basis to

## 1. Introduction

Lithium-ion batteries (LIBs) feature excellent electrochemical properties, e.g., high energy density and cycling stability, and are widely used in consumer electronics and electric transportation. Despite the favorable properties of LIB, the production process can still be improved.<sup>[1]</sup> One approach is to decrease the production costs in electrode production through new production processes.<sup>[2]</sup> Conventional electrode production consists mainly of the process steps mixing, coating, drying, and

M. Leeb, N. Schwarz, R. Daub  
Technical University of Munich  
TUM School of Engineering and Design  
Institute for Machine Tools and Industrial Management iwB  
Boltzmannstr. 15, 85748 Garching, Germany  
E-mail: matthias.leeb@iwB.tum.de

R. Daub  
Fraunhofer Institute for Casting, Composite and Processing  
Technology (IGCV)  
Am Technologiezentrum 10, 86159 Augsburg, Germany

The ORCID identification number(s) for the author(s) of this article can be found under <https://doi.org/10.1002/ente.202401759>.

© 2024 The Author(s). Energy Technology published by Wiley-VCH GmbH. This is an open access article under the terms of the Creative Commons Attribution-NonCommercial License, which permits use, distribution and reproduction in any medium, provided the original work is properly cited and is not used for commercial purposes.

DOI: 10.1002/ente.202401759

model and predicted electrode properties within the process, which ultimately leads to a digital twin.

The aim of this study was to analyze the film formation process and its effects on the electrode properties for the semidry anode production. Electrode properties in the film formation step were varied at several calender gaps and roller speeds. Compared to previous studies, this study focused on the calendaring step instead of the extrusion step. In a conducted preliminary study, the relevant process parameters were identified and a parameter window for a subsequent experimental design was determined. The roller speed was varied up to  $4 \text{ m min}^{-1}$  instead of a fixed roller speed of  $0.2 \text{ m min}^{-1}$  and the calender gap was varied to produce different mass loadings. Hence, the influence of the calender parameters, particularly roller speed and calender gap, on the electrode properties were identified. The analyzed electrode properties were divided into geometric properties, electrochemical properties, microstructure, and mechanical properties.

## 2. Results and Discussion

### 2.1. Determination of a Parameter Window

In dry coating, free-standing films were produced using differential speed between the rollers to induce shear forces during film formation.<sup>[15]</sup> The differential speed used induces an asymmetrical force on the granules within the calender gap.<sup>[16]</sup> In semidry electrode production, however, low differential speed of 10% between roller 1 and 2 resulted in an uneven coating and led to a ripping of the current collector foil. The applied shear force within the gap causes a high tension on the current collector and the release foil. Differential speed was found to be not feasible with this semidry electrode production process and all roller speeds were set to the same speed for the study. In semidry electrode production, the release foil had a different friction coefficient compared to the current collector foil, inducing an asymmetrical force within the calender gap.

As expected, the first gap had a significant influence on the film thickness and mass loading of the electrode.<sup>[17]</sup> Additionally, the roller speed had a significant effect on the mass loading and thickness of the electrode. In **Figure 1**, a positive correlation between the calender gap and the mass loading of

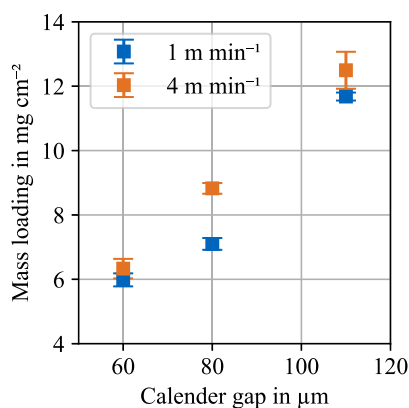


**Figure 1.** Electrode mass loading over the calender gap at the roller speeds of 1 and  $4 \text{ m min}^{-1}$ .

the electrode is visible. Based on the literature, the positive correlation of the calender gap was expected.<sup>[18]</sup> Also, the electrodes produced at higher speed tended to have higher mass loading. The roller speed influence may be caused by the fact that the friction coefficients between granules and rollers are dependent on the shear forces and the roller speed. Therefore, the material feeding into the calender gap is different.

A homogeneous distribution of sodium in the electrode cross section showed no binder migration despite the change in drying time due to the varying roller speed up to  $4 \text{ m min}^{-1}$  in the semidry electrode production (see Figure S1, Supporting Information). The element sodium is found in the carboxymethyl cellulose (CMC) binder which indicates the binder distribution within the electrode and is utilized to identify binder migration.<sup>[19,20]</sup> These results proved that no binder migration was taking place at the semidry electrode production.

In **Figure 2**, the influence of the granule size on the relative mass loading and the density of the electrode in the film formation is shown. Larger granules corresponded to a granule length of around 1 mm and small granules were in the range of 0.5 mm. For the relative mass loading calculation, the electrodes produced with 0.5 mm granules were set as baseline. Figure 2a depicts a higher relative mass loading of about 6–12% when using large granules instead of small granules. As shown in Figure 2b, the electrode density was higher with a value of  $1.35 \text{ g cm}^{-3}$  compared to around  $1.31 \text{ g cm}^{-3}$  when using larger granules. For further analysis of the film formation process, the small granules with a length of 0.5 mm were utilized, as the finer granules led to a more homogenous visual electrode surface. Overall, the density after the film formation process is higher compared to the electrode density resulting from the conventional coating process with identical mass loading with  $1 \text{ g cm}^{-3}$ .<sup>[7]</sup>

### 2.2. Experimental Design

#### 2.2.1. Geometric Properties

**Figure 3** illustrates the electrode thickness, the mass loading, and the porosity of the produced electrodes at a roller speed of  $2 \text{ m min}^{-1}$ . The electrode thickness and the mass loading had a strong linear correlation except for the data point at a calender gap of  $70 \mu\text{m}$ . The data point could be caused by slightly larger granules in the calendaring gap or a thickness variation in the release foil. A thickness variation of the release foil seemed rather unlikely. A strong correlation is expected and in agreement with the existing literature.<sup>[18]</sup> The thickness of the electrode was  $\approx 5\text{--}10 \mu\text{m}$  lower than the calendaring gap. The mass loading ranged from  $\approx 7$  to  $14 \text{ mg cm}^{-2}$ . The porosity of the electrode remained relatively constant for small calender gaps but tended to decrease for larger ones. To give a comprehensive overview of the experiment data, a correlation analysis was performed on the dataset.

**Figure 4a** depicts the correlation matrix of the dataset between the process parameters on the abscissa and the product parameters on the ordinate. Each tile in the correlation matrix represents the Pearson correlation coefficient (PCC) and  $p$ -value in brackets between individual process parameters and geometric properties. The process parameters were considered statistically independent. The correlation matrix exhibits a strong positive correlation of the calender gap on the electrode thickness

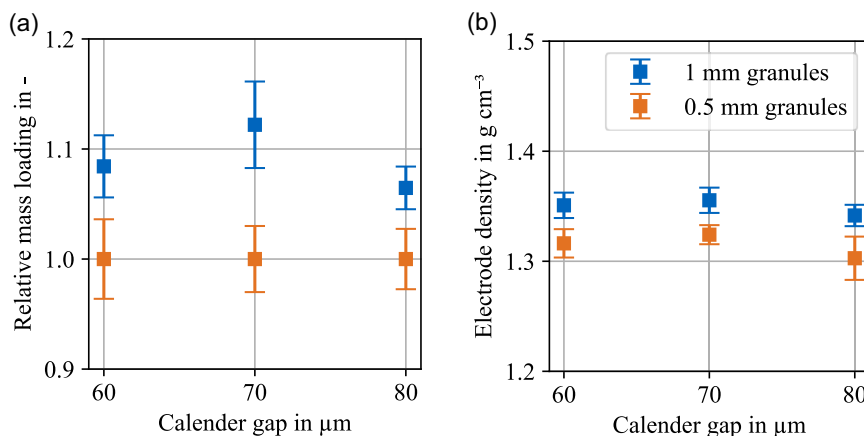


**Figure 2.** a) Influence of granule size on electrode mass loading and b) on electrode density.

and the mass loading. A moderate negative correlation of the calender gap with the porosity was found. All three correlations were significant as the  $p$ -value was 0.00. This result is in good agreement with the results in Figure 2. A scatter plot of the complete dataset for the electrode thickness is provided in Figure S2, Supporting Information. The roller speed was found to have no significant linear correlation with the electrode properties.

In Figure 4b, the electrode thickness and the mass loading over the roller speed at a calender gap of  $90\ \mu\text{m}$  are shown. The data indicated a nonlinear correlation between the roller speed and the electrode thickness as well as the mass loading of the electrode. The nonlinear correlation explained why the correlation matrix indicated no significant linear correlation

between the roller speed and the electrode properties. The effect of the speed dependency was not investigated in the literature so far and should be included in future studies with an adapted speed range. The speed dependency is probably caused by a change in friction coefficients between the granules and current collector and release foil at different speeds. A change in the friction coefficient causes a change in the nip angle and defines ultimately the compaction ratio of the granules.<sup>[21]</sup>

### 2.2.2. Electrochemical Properties

The effect of the process and the product parameters of the calendering process on the ionic resistance, the tortuosity, and the

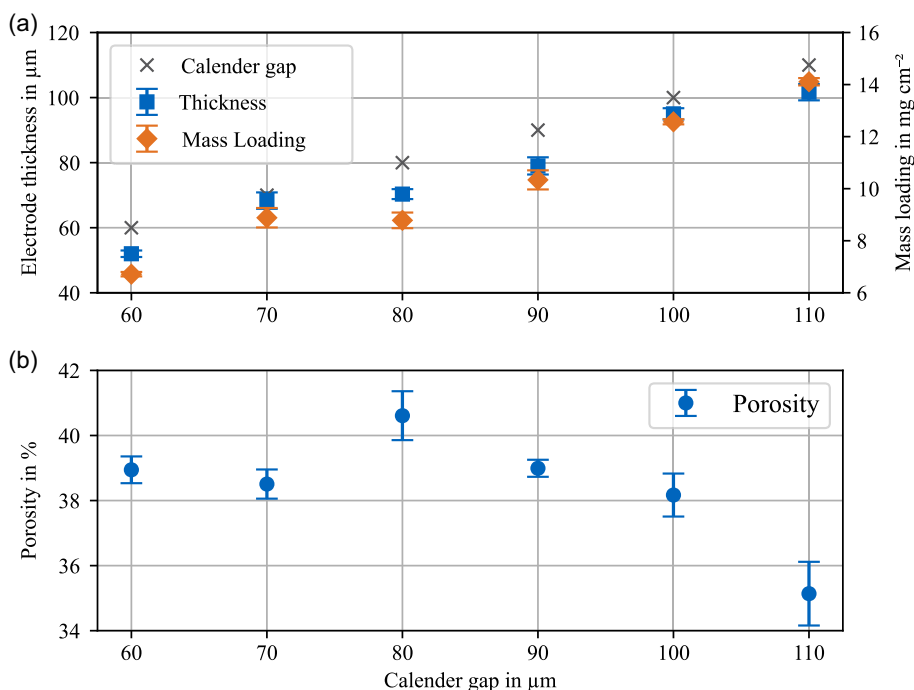


**Figure 3.** Geometric properties of the produced electrodes with a roller speed of  $2\ \text{m min}^{-1}$ . a) The electrode thickness and the mass loading correlate linearly with the calender gap. The electrode thickness tends to be  $5\text{--}10\ \mu\text{m}$  lower than the calender gap. b) The porosity decreased at larger calender gaps.

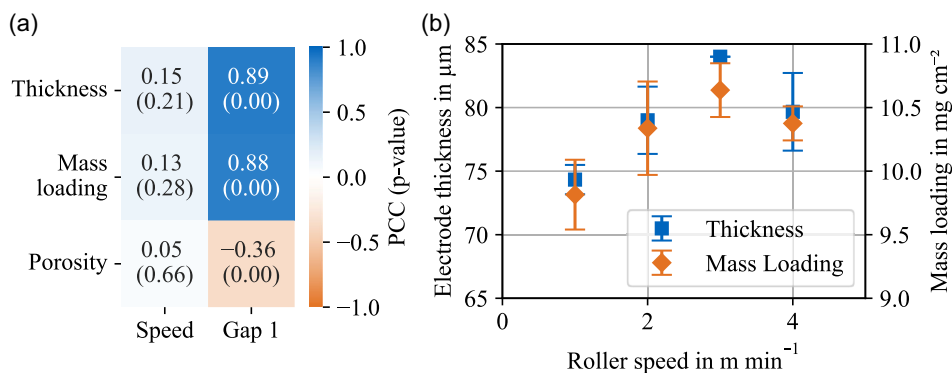


**Figure 4.** a) Correlation matrix between process parameters (roller speed, calender gap) and electrode properties. b) Electrode thickness and mass loading over the roller speed at a calender gap of 90 μm.

McMullin number are displayed in the correlation matrix in **Figure 5**. The roller speed significantly influences the electrochemical properties of the anodes. The ionic resistance, the tortuosity, and the McMullin number decreased with the increasing roller speed. This indicates that the roller speed influences the film formation of the semidry anode production. A significant positive correlation of the calender gap on the ionic resistance was found, which means that a larger gap increases the ionic resistance mainly due to the increase in the mass loading and the thickness of the electrode. The tortuosity and McMullin number were mostly unaffected by the calender gap and as these values are normalized by the thickness. A scatter plot of the speed dependency for the ionic resistance and the tortuosity is provided in **Figure S4**, Supporting Information.

To further analyze and confirm the results of the correlation matrix regarding the dependence of the speed on the electrochemical properties, additional symmetrical cells at a constant mass loading were assembled. All electrode had the same mass loading of 10.5 mg cm<sup>-2</sup> and a porosity of 38%, which were produced at different roller speeds between 1 and 4 m min<sup>-1</sup> at film formation. A conventionally wet-coated reference with a porosity of around 40% was also analyzed. **Figure 6** depicts the ionic resistance of the anodes, in which a decrease of the ionic resistance at a constant porosity of around 38% was determined. The semidry produced anodes with lower porosity had a decreased ionic resistance, compared to the wet-coated reference anode, which was also shown in the literature.<sup>[22]</sup> The standard deviation of the porosity is mostly lower than 0.5% except for the data point at

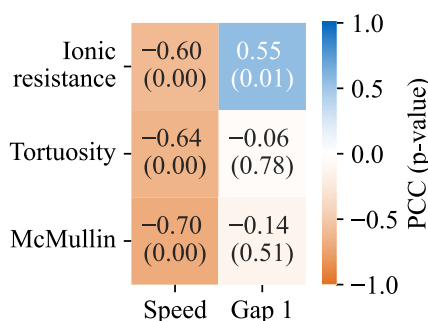


**Figure 5.** Correlation of process parameters and mass loading on the ionic resistance, the tortuosity, and the McMullin number.

2 m min<sup>-1</sup>. Despite the high standard deviation of around 1%, the standard deviation for the ionic resistance was similar to the other roller speeds, which indicated a larger speed influence compared to the influence of the porosity. This result is in agreement with the findings of Wiegmann et al. who found that the semidry electrodes exhibited higher discharge capacities at high C-rates.<sup>[7]</sup> The speed influence shows also that the ionic resistance can be optimized based on the process parameters in the film formation process, which will be analyzed further in future work.

### 2.2.3. Scanning Electron Microscopy Analysis

Usually, the particle distribution and the homogeneity of the electrode are affected by different mixing parameters. In this study, the parameters for the granule extrusion and the granule recipe were kept constant, so differences resulting from the roller speed should be visible. Regarding the microstructure, no clear trend could be seen on the surface of the electrode, but there were residues, which can be seen in the top row in **Figure 7**. Further analysis showed that these were residues from the silicone-coated release foil used to avoid electrode adhesion on the second roller. The residues are labeled with red rectangles and decreased in size as the roller speed increased. The residue

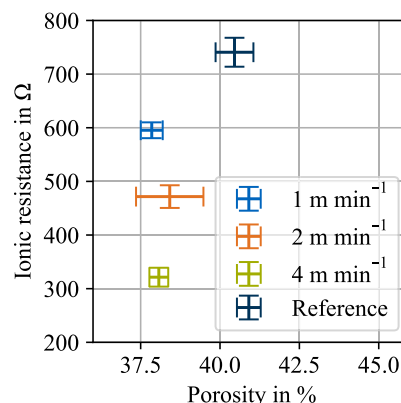


**Figure 6.** The ionic resistance at a mass loading of 10.5 mg cm<sup>-2</sup> and similar electrode porosity is lower at higher roller speed. The conventionally coated reference electrode was found the highest resistance despite higher porosity.

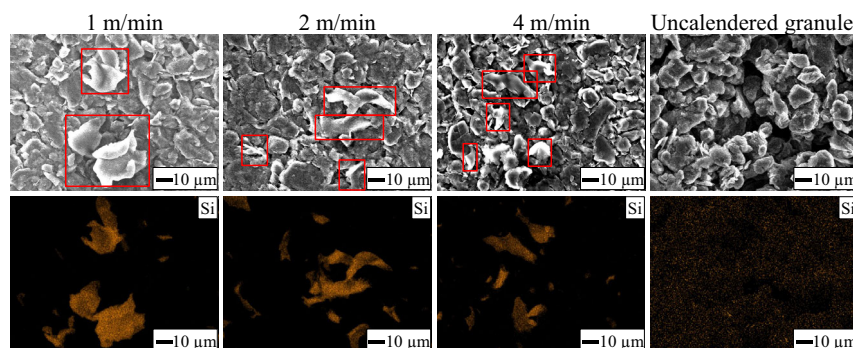


**Figure 7.** SEM (top) and EDXS (bottom) images of silicone residues on the electrode surface for different roller speeds and the uncalendered granule. The red rectangles depict residues. At lower roller speeds the silicone residues were larger, which was validated with the EDXS maps at the bottom.

size was correlated with the contact time of the electrode and the release foil within the gap. On the uncalendered granules, no silicone residues could be found on the electrode surface.

A clear indication of the silicone residues is the energy-dispersive X-ray spectroscopy (EDXS) analysis using the silicon map shown at the bottom in Figure 7. The silicone residues from the used release foil can be identified and correlated with the scanning electron microscopy (SEM) images above. The oxygen map reveals analog behavior, which further proves the presence of silicone residues. The distribution of carbon is shown in Figure S5, Supporting Information. Silicone is a polymer, which consists of chains of the elements silicon and oxygen with additional organic groups. The granules likewise indicated silicon content, but it is evenly distributed within the electrode and at lower concentration. The silicon content for the granules was attributed to the nitrile butadiene rubber (NBR) binder, which is used in the electrode. Silicon dioxide is utilized as additive in NBR to improve the rheological and mechanical properties.<sup>[23,24]</sup>

The silicone residues were not homogeneously distributed on the surface of the electrodes (see Figure S6, Supporting Information). Although the relative intensities were low, there were large and noticeable residuals present on the surfaces. The results of the quantitative analysis of the silicon contents are summarized in Table 1. The relative silicon content was less than 1% and was decreasing with higher roller speed. The increase from 0.57% at 1 m min<sup>-1</sup> to 0.64% at 2 m min<sup>-1</sup> can be explained by stochastic effects as the residues are not homogeneously distributed and form large clusters. The uncalendered granules without contact to the release foil showed the lowest silicone content, which can be attributed to the NBR binder.

As the silicone residues and the electrochemical properties showed a similar trend, one could conclude that this is the reason

**Table 1.** Surface silicon content at different roller speeds.

Roller speed [m min <sup>-1</sup> ]	Relative silicon content [%]
1	0.57
2	0.64
3	0.33
4	0.29
Uncalendered granule	0.10

for the change in ionic resistance and tortuosity. Nevertheless, the relative silicon content was less than 1%. Despite the silicone residues, which potentially increase the ionic resistance, the semidry produced electrodes showed better electrochemical performance than the conventionally produced reference electrode.

#### 2.2.4. Mechanical Electrode Properties

The correlation matrix between the process parameters and mechanical electrode properties is depicted in Figure 8. The first calender gap was moderately, negatively correlated with the reduced elastic modulus and the hardness of the electrodes. The correlation analysis between the calender gap and the fraction of elastic deformation energy exhibited statistical significance and a weak correlation, which can be explained with the thicker electrode. The speed has a statistically significant effect on the reduced elastic modulus and the hardness of the electrodes, which exhibited a weak negative relationship. A previous study investigating the effect of the calendaring speed on the density of conventional lithium nickel manganese cobalt oxide (NMC) and graphite electrodes showed that a lower calendaring speed led to a higher density of both the NMC and graphite electrodes.<sup>[25]</sup> At lower speed, the material undergoes the calendaring between the rollers for a longer time, which may lead to a more efficient arrangement of the particles, and therefore a higher hardness and reduced elastic modulus. However, no significant correlation between the roller speed and the porosity of the electrodes could be identified in this study. An alternative explanation could be the silicone residues on the surface of the electrode

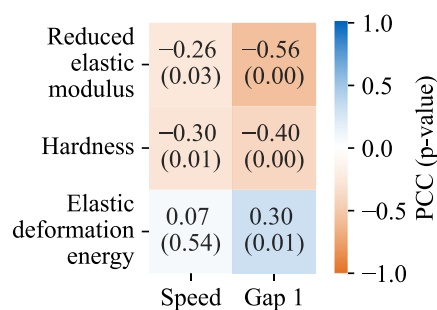


**Figure 8.** Correlation matrix between process parameters and mechanical properties of the semidry produced anodes.

as the reduced elastic modulus and the hardness are evaluated at the peak force during indentation and the silicone is softer than the electrode particles. Therefore, the hardness and the reduced elastic modulus decreased slightly. A scatter plot of the speed dependency for the reduced elastic modulus and the hardness is provided in Figure S8, Supporting Information. The fraction of the elastic deformation energy which was calculated over the whole displacement curve indicated no correlation with the roller speed. This supports the assumption that there was a change in the electrode surface.

### 3. Conclusion

In this study, the cause–effect relationships of the film formation between the process parameters and the electrode properties in the semidry electrode production process were analyzed. Different process parameters were investigated and condensed to a final set of parameters for the experimental design. Experiments showed that in the semidry process differential roller speeds were not feasible, as the current collector ripped within the gap. Based on the drying constraint, the maximum speed at which the electrode can be dried was found to be  $4 \text{ m min}^{-1}$ . Larger granules within the calender gap resulted in higher mass loading and higher electrode density. The calender gap showed the strongest correlation on the mass loading and thickness. Contrary to the literature, a strong positive correlation of the roller speed on the geometric properties was identified. The speed dependency was pronounced at small calender gaps, but not statistically significant at larger calender gaps. Additionally, semidry electrodes exhibited significantly reduced ionic resistance compared to a conventionally produced anode. The resistance decreased with increased roller speed. The detected residues of the silicone-coated release foil on the surface of the electrodes may cause these observations. Nevertheless, the total amount of residues on the electrode surface was less than 1%. The nanoindentation measurements supported the explanation of a surface effect for the decrease in ionic resistance. More investigation is needed to understand and explain this phenomenon. In summary, this study demonstrates the correlation of the calender gap and the roller speed on the properties of semidry produced anodes. The roller speed moderately influenced the geometric electrode properties, but strongly influenced the ionic resistance. The choice of the release foil has to be considered in the semidry electrode production regarding possible residues.

Further research should be done on the electrochemical properties, e.g., the analysis of different release foils and the optimization of ionic resistance within the electrode. Furthermore, the effect of granule size on the electrode properties should be quantified.

### 4. Experimental Section

**Materials:** Graphite active material (SGL Carbon, Germany) and conductive carbon black SC65 (Imerys, France) were used to produce the anode. The water-soluble CMC (2000PA, Dow, USA) was utilized as binder in combination with the NBR (Nanoprene M20OH VP, Arlanxeo, The Netherlands) or styrene-butadiene rubber (SBR) (BM-451B, Zeon, Germany). The anode was coated onto a  $10 \mu\text{m}$  copper foil (Sumitomo

**Table 2.** Material formulation of the processed anodes and material densities.

	Mass fraction semidry [wt%]	Mass fraction reference [wt%]	Density [ $\text{g cm}^{-3}$ ]
Graphite	93.00	93.00	2.26
Carbon black	1.40	1.40	2.00
CMC	1.87	1.87	1.60
SBR	–	3.73	1.04
NBR	3.73	–	0.94

Metal Mining, Japan). All tests regarding anodes carried out within this work were based on the formulation given in **Table 2**. Furthermore, a silicone-coated paper (B 650 weiss, Laufenberg, Germany) was used as release foil.

**Granule Preparation:** A twin-screw extruder (RheomexPTW16/40 OS, Thermo Fischer, Germany) and a strand granulator (hot die cutting HAAKE PolyLab OS, Thermo Fischer, Germany) were used to produce the granules. All powders were premixed with the binder and fed within the extruder at a feed rate of  $0.612 \text{ kg h}^{-1}$ . Deionized water was added as solvent with  $0.188 \text{ kg h}^{-1}$ , resulting in a solid content of 76.5%. The granules were stored airtight in small containers and opened right before the coating/calendering process. The granule size was controlled with the cutting speed of the strand granulator ( $20$  and  $40 \text{ s}^{-1}$ ) and was determined using a ruler.

**Coating/Calendering:** Relevant process parameters like the calender gap, roller speed, and roller temperatures as well as granule properties for the semidry electrode production were identified in a previous study.<sup>[17]</sup> The roller diameter was fixed in the four-roller calender at a diameter of  $200 \text{ mm}$ . In addition, the anode granule formulation based on Wiegmann et al. was kept constant as several iterative improvements of the granule formulation were already included.<sup>[17]</sup> In **Figure 9**, a four-roller calender (Saueressig, Germany) with the rollers arranged horizontally, forming three calender gaps is illustrated. The current collector and the release foil were placed accordingly. In the first gap between roller 1 and 2, the granules were fed along with the current collector and pressed onto it. The release foil prevented any adhesions from the granules onto roller 2 and was separated from the electrode after the second gap. This was considered as the film formation process, which was the focus of this study. The third calender gap was kept constantly open for this study.

The first two rollers were set at room temperature of  $\approx 20 \text{ }^\circ\text{C}$  to prevent the evaporation of the solvent in the granules in contact with the rollers. Drying of the granules before film formation resulted in a bridge film and coating defects, and was therefore excluded. Rollers 3 and 4 were each set at  $60 \text{ }^\circ\text{C}$  to dry the electrode film through thermal conduction in contact with the rollers, which was kept constant during the study. Based on the defined temperature settings, the process parameter window in terms of roller speed was determined. Up to a calender gap of  $110 \mu\text{m}$  and a roller speed of  $4 \text{ m min}^{-1}$ , the anode was dry enough for further processing. During electrode production, the calender gap was set and the granules were fed into the first calender gap. A single-sided coated electrode, with a length of at least  $20 \text{ cm}$  for each gap setting and an electrode width of  $10 \text{ cm}$ , was produced with the desired roller speed.

**Experimental Design:** Based on the acquired parameter window for the semidry film formation process defined in the previous section, an experimental design was set up to identify the cause–effect correlations of the process parameters speed and gap 1 on the electrode properties. The electrode properties will be evaluated in terms of geometrical properties, namely, the mass loading, the thickness, and the porosity, additionally microstructural and electrochemical properties were considered. **Table 3** summarizes the process parameter variations in the partial factorial experimental design. The roller speed was varied from  $1$  to  $4 \text{ m min}^{-1}$ ; the calender gap 1 was varied between  $60$  and  $110 \mu\text{m}$ . This experimental design results in a total of 24 different experiments. The calender gap of  $60 \mu\text{m}$

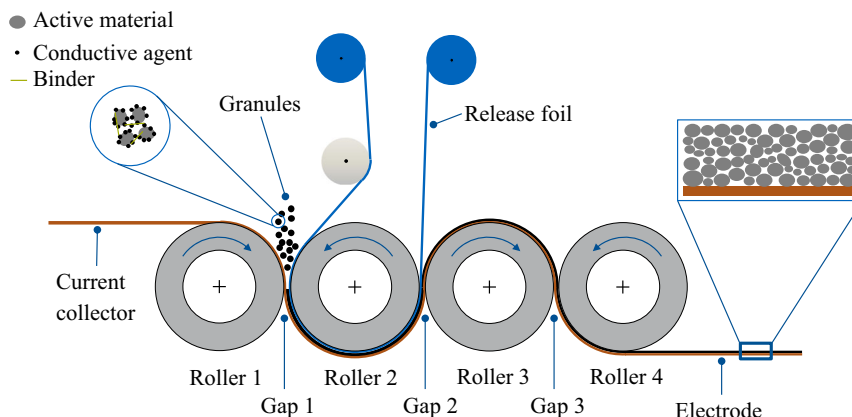


**Figure 9.** Schematic illustration of a four-roller calender to form a semidry-produced electrode.

**Table 3.** Summary of the chosen process parameter levels for the experimental design.

Process parameter	Levels
Roller speed [ $\text{m min}^{-1}$ ]	[1, 2, 3, 4]
Calender gap 1 [ $\mu\text{m}$ ]	[60, 70, 80, 90, 100, 110]

corresponds to a gap width of  $0 \mu\text{m}$ , as the  $10 \mu\text{m}$  thick copper foil and the  $50 \mu\text{m}$  thick release foil reducing the gap width. The second calender gap was identical to gap 1. Tests with the second calender gap  $10 \mu\text{m}$  smaller than the first calender gap indicated a slight but no significant difference in the electrode thickness.

**Electrode Properties:** After the film formation process, the electrodes were post-dried in a vacuum oven at  $80^\circ\text{C}$  for 8 h before measuring the weight and the electrode thickness. Six samples with a diameter of 15 mm were punched out of each electrode segment along with two further samples from the uncoated copper foil, resulting in eight samples in total. The electrode and copper foil weights were measured with a microbalance (Mettler Toledo, Switzerland), and the thicknesses were measured with a digital indicator (Mitutoyo, Japan). The mass loading was calculated as the fraction of the coating mass and the area of the sample. The difference between the electrode and the foil thickness referred to the coating thickness. To determine electrode density, the quotient of the mass loading and the electrode thickness was used. The porosity of the electrode was calculated using the electrode density  $\rho_{\text{electrode}}$  and the true density of the materials used according to Equation (1). Using the material mass fractions  $w_i$  and the material densities  $\rho_i$  in Table 2, the true density of the formulation was calculated using Equation (2):

$$\text{Porosity} = 1 - \frac{\rho_{\text{electrode}}}{\rho_{\text{true density}}} \quad (1)$$

$$\rho_{\text{true density}} = \left( \sum_i \frac{w_i}{\rho_i} \right)^{-1} \quad (2)$$

**Cell Preparation:** Symmetrical coin cells were manufactured under dry room atmosphere at a dew point of around  $-40^\circ\text{C}$ . Electrochemical impedance spectroscopy was used to characterize the anodes. Two anode samples of diameter 15 mm and a maximum deviation in mass of 1.0% and in thickness of 1.5%, respectively, were matched per cell. The casing of the coin cells consisted of a bottom casing, a top casing, a spring, and two metal plates of thicknesses 1 and 0.5 mm.  $100 \mu\text{L}$  of non-intercalating electrolyte and a glass fiber separator (VWR, Germany) was placed between the anode samples. The electrolyte was composed of 100 mmol

tetrabutylammonium perchlorate dissolved in ethylene carbonate and methyl carbonate with a ratio of 3:7.

**Electrochemical Impedance Spectroscopy:** The tests were performed using an impedance spectroscopy (VSP-3e, BioLogic, France). The cells were tested within a climate chamber at a constant temperature of  $25^\circ\text{C}$ . A frequency range between 100 mHz and 10 kHz was used to measure the impedance spectrum. The experimental data were fitted using the transmission line model developed by Landesfeind et al.<sup>[26]</sup> and the electrode parameters were extracted accordingly. The tortuosity was defined as the quotient of the shortest pathway through a porous structure and the Euclidean distance between the starting and end point of that pathway.<sup>[27]</sup> Additional elements were added to the equivalent circuit to account for the additional impedances in the electrode, like the separator and the contact impedances. The electrical parameters represent averages of the two anodes in the coin cell. The determined values for the ionic resistance and the tortuosity were considered to be representative of both anodes as the two anodes had the same properties. The applied equivalent circuit is given in Figure S3, Supporting Information.

**Correlation Analysis:** The PCC describes the degree of linear correlation between two variables. By definition, the PCC can assume values between  $-1$  and  $1$ . A PCC of 0 indicates no linear correlation, a positive PCC indicates a positive linear correlation, and a negative PCC indicates a negative linear correlation. Absolute PCC values between 0 and  $\pm 0.3$  represent a weak correlation, while absolute PCC values above 0.7 indicate a strong linear correlation.<sup>[28]</sup> The PCC for two variables can be calculated based on the covariance (COV) between the two variables and the standard deviations  $\sigma_x$  and  $\sigma_y$  of the two variables:

$$\text{PCC} = \frac{\text{COV}(x,y)}{\sigma_x \sigma_y} \quad (3)$$

Using a null hypothesis test based on the analysis of variance, the  $p$ -value for a relationship between two variables is calculated.<sup>[29]</sup> The  $p$ -value displays the degree of the relationship against a null hypothesis, which claims that there is no relationship between the variables. A  $p$ -value below 0.05 indicates statistical significance.<sup>[30]</sup>

**SEM Analysis:** SEM and EDXS images were taken using a SEM (JSM-IT200 InTouchScope, JEOL, Japan) at an acceleration voltage of 15 kV. SEM images of the electrode surface were taken to analyze the microstructure and the residues on the surface of the electrodes. EDXS images were used to investigate the silicon and oxygen map of the electrode surface to identify the silicone residues. To compare a coating with and without using the silicone-coated release film, the uncalendered granules was analyzed. Therefore, granules were pressed manually by hand between two copper foils while the upper foil was rotated and sheared against the coating to avoid adhesion on the upper foil. To quantify the residue amount on the electrode surface, an EDXS analysis was performed using a magnification

of 100x, which correlates to an area of 1 mm<sup>2</sup>. The EDXS sodium map was used to identify the homogeneity of the CMC binder in the electrode cross section. Sodium is an element in the CMC binder.

**Nanoindentation:** The physical properties of the electrode were tested using nanoindentation with a flat punch with a diameter of 100 μm (UNAT nanomechanical tester by ASMEC, ZwickRoell, Germany). Displacement-controlled measurements were conducted at varying indentation depths of 10, 20, and 30 μm. For all testing sequences, the loading and unloading rates were constant at 150 nm s<sup>-1</sup>.<sup>[31]</sup> Prior to measuring each sample, a surface approach test followed by a thermal drift correction test was conducted to avoid time-dependent errors due to thermal expansion.<sup>[32]</sup> For each depth, 49 indentations were conducted. The reduced elastic modulus and the hardness as well as the fraction of the elastic deformation energy were evaluated to gain further insights into the microstructure of the electrode. The characteristic values used for the detection of outliers were the elastic modulus, the maximal force used, and the indentation depth at the maximal force. An example indentation is depicted in Figure S7, Supporting Information. The contact stiffness between the indenter and the material is defined as the initial load–displacement slope of the unloading phase, and the hardness of the material as the ratio between the maximum indentation load and the contact area of the indentation.<sup>[33]</sup> The reduced elastic modulus is calculated using the ratio of the contact stiffness to the contact area.<sup>[34]</sup> The fraction of the elastic deformation energy is defined the quotient of elastic deformation energy calculated from the unloading phase and the total deformation energy calculated from the loading phase.

## Supporting Information

Supporting Information is available from the Wiley Online Library or from the author.

## Acknowledgements

The authors express their gratitude to the German Federal Ministry of Education and Research (BMBF) for the funding of the research and to the project management Julich (Ptj) for coordinating the project. The results presented in the article have been acquired within the scope of the research project “GranuProd” (O3XP0344B).

Open Access funding enabled and organized by Projekt DEAL.

## Conflict of Interest

The authors declare no conflict of interest.

## Author Contributions

**Matthias Leeb:** Conceptualization; Methodology; Investigation; Visualization; Writing—original draft; Writing—review and editing.  
**Nico Schwarz:** Investigation; Writing—original draft. **Rüdiger Daub:** Funding acquisition; Supervision; Writing—review and editing.

## Data Availability Statement

The data that support the findings of this study are available from the corresponding author upon reasonable request.

## Keywords

calendering, electrode production, lithium-ion batteries, semidry, solvent-reduced

Received: September 12, 2024  
Revised: October 4, 2024  
Published online: November 17, 2024

- [1] F. Duffner, L. Mauler, M. Wentker, J. Leker, M. Winter, *Int. J. Prod. Econ.* **2021**, 232, 107982.
- [2] F. Degen, O. Krätzig, *IEEE Trans. Eng. Manage.* **2024**, 71, 1038.
- [3] A. Kwade, W. Haselrieder, R. Leithoff, A. Modlinger, F. Dietrich, K. Droeder, *Nat. Energy* **2018**, 3, 290.
- [4] D. Griebel, A. Adam, K. Huber, A. Kwade, *J. Electrochem. Soc.* **2022**, 169, 20531.
- [5] Y. Liu, R. Zhang, J. Wang, Y. Wang, *iScience* **2021**, 24, 102332.
- [6] S. N. Bryntesen, A. H. Strømman, I. Tolstorebrov, P. R. Shearing, J. J. Lamb, O. Stokke Burheim, *Energies* **2021**, 14, 1406.
- [7] E. Wiegmann, A. Kwade, W. Haselrieder, *Energy Technol.* **2022**, 10, 2200020.
- [8] P. Mitchell, X. Xi, L. Zhong, US Patent 7,883,553 B2 **2008**.
- [9] E. Wiegmann, S. Fischer, M. Leeb, A. Kwade, *Batteries* **2023**, 9, 567.
- [10] Y. Lu, C.-Z. Zhao, H. Yuan, J.-K. Hu, J.-Q. Huang, Q. Zhang, *Matter* **2022**, 5, 876.
- [11] M. F. V. Hidalgo, G. Apachitei, D. Dogaru, M. Faraji-Niri, M. Lain, M. Copley, J. Marco, *J. Power Sources* **2023**, 573, 233091.
- [12] S. Haghi, J. Keilhofer, N. Schwarz, P. He, R. Daub, *Batteries Supercaps* **2024**, 7, e202300457.
- [13] S. X. Drakopoulos, A. Gholamipour-Shirazi, P. MacDonald, R. C. Parini, C. D. Reynolds, D. L. Burnett, B. Pye, K. B. O'Regan, G. Wang, T. M. Whitehead, G. J. Conduit, A. Cazacu, E. Kendrick, *Cell Rep. Phys. Sci.* **2021**, 2, 100683.
- [14] E. N. Primo, M. Touzin, A. A. Franco, *Batteries Supercaps* **2021**, 4, 834.
- [15] B. Schumm, S. Kaskel, *Next Energy* **2023**, 1, 100009.
- [16] D. Pustovoytov, A. Pesin, P. Tandon, *Metals* **2021**, 11, 956.
- [17] M. Leeb, E. Wiegmann, A. Kwade, R. Daub, *Procedia CIRP* **2023**, 120, 732.
- [18] K. M. Moroney, P. Cronin, O. A. Adeleye, B. E. Schaller, M. A. Howard, B. Castro-Dominguez, R. Ramachandran, G. M. Walker, *Powder Technol.* **2020**, 366, 82.
- [19] B. Westphal, H. Bockholt, T. Günther, W. Haselrieder, A. Kwade, *ECS Trans.* **2015**, 64, 57.
- [20] S. Jaiser, N. Sanchez Salach, M. Baunach, P. Scharfer, W. Schabel, *Drying Technol.* **2017**, 35, 1807.
- [21] J. R. Johanson, *J. Appl. Mech.* **1965**, 32, 842.
- [22] E. Wiegmann, H. Cavers, A. Diener, A. Kwade, *Energy Technol.* **2023**, 11, 2300341.
- [23] M. Hussain, S. Yasin, H. Memon, Z. Li, X. Fan, M. A. Akram, W. Wang, Y. Song, Q. Zheng, *Polymers* **2020**, 12, 2763.
- [24] N. Z. Noriman, H. Ismail, *J. Appl. Polym. Sci.* **2012**, 124, 19.
- [25] C. Meyer, H. Bockholt, W. Haselrieder, A. Kwade, *J. Mater. Process. Technol.* **2017**, 249, 172.
- [26] J. Landesfeind, J. Hattendorff, A. Ehrl, W. A. Wall, H. A. Gasteiger, *J. Electrochem. Soc.* **2016**, 163, A1373.
- [27] B. Tjaden, D. J. L. Brett, P. R. Shearing, *Int. Mater. Rev.* **2018**, 63, 47.
- [28] B. Ratner, *J. Targeting Meas. Anal. Mark.* **2009**, 17, 139.
- [29] L. Stähle, S. Wold, *Chemom. Intell. Lab. Syst.* **1989**, 6, 259.
- [30] S. Goodman, *Semin. Hematol.* **2008**, 45, 135.
- [31] D. Schreiner, J. Lindenblatt, R. Daub, G. Reinhart, *Energy Technol.* **2023**, 11, 2200442.
- [32] J. M. Wheeler, D. E. J. Armstrong, W. Heinz, R. Schwaiger, *Curr. Opin. Solid State Mater. Sci.* **2015**, 19, 354.
- [33] *Springer EBooks Engineering* (Eds: S. Schmauder, C.-S. Chen, K. K. Chawla, N. Chawla, W. Chen, Y. Kagawa), Springer, Singapore **2019**.
- [34] M. L. Oyen, R. F. Cook, *J. Mech. Behav. Biomed. Mater.* **2009**, 2, 396.